AFRL-RX-WP-JA-2016-0274

AN EBSD INVESTIGATION OF ULTRAFINE-GRAIN TITANIUM FOR BIOMEDICAL APPLICATIONS (POSTPRINT)

G.S. Dyakonov and I.P.Semenova
Ufa State Aviation Technical University

G.S. Dyakonov, E.Zemtsova, and R.Z.Valiev
Saint Petersburg State University

S.Mironov
Tohoku University

S.L. Semiatin
AFRL/RX

15 JULY 2015
Interim Report

AIR FORCE RESEARCH LABORATORY
MATERIALS AND MANUFACTURING DIRECTORATE
WRIGHT-PATTERSON AIR FORCE BASE, OH 45433-7750
AIR FORCE MATERIEL COMMAND
UNITED STATES AIR FORCE

REPORT DOCUMENTATION PAGE

Form Approved
OMB No. 0704-0188

1. REPORT DATE *(DD-MM-YY)*	2. REPORT TYPE	3. DATES COVERED *(From - To)*
15 July 2015	Interim	19 March 2014 – 15 June 2015

4. TITLE AND SUBTITLE
AN EBSD INVESTIGATION OF ULTRAFINE-GRAIN TITANIUM FOR BIOMEDICAL APPLICATIONS (POSTPRINT)

5a. CONTRACT NUMBER
IN-HOUSE

5b. GRANT NUMBER

5c. PROGRAM ELEMENT NUMBER

6. AUTHOR(S)
1) G.S. Dyakonov and I.P.Semenova - Ufa State Aviation Technical University
2) G.S. Dyakonov, E.Zemtsova, and R.Z.Valiev – St. Petersburg State University
(continued on page 2)

5d. PROJECT NUMBER

5e. TASK NUMBER

5f. WORK UNIT NUMBER
X0W6

7. PERFORMING ORGANIZATION NAME(S) AND ADDRESS(ES)
1) Ufa State Aviation Technical University, 12K Marx St., Ufa 450000, Russia
2) St. Petersburg State University
26 Universitetsky Prospect
198504 Peterhof
St. Petersburg, Russia
(continued on page 2)

8. PERFORMING ORGANIZATION REPORT NUMBER

9. SPONSORING/MONITORING AGENCY NAME(S) AND ADDRESS(ES)
Air Force Research Laboratory
Materials and Manufacturing Directorate
Wright-Patterson Air Force Base, OH 45433-7750
Air Force Materiel Command
United States Air Force

10. SPONSORING/MONITORING AGENCY ACRONYM(S)
AFRL/RXCM

11. SPONSORING/MONITORING AGENCY REPORT NUMBER(S)
AFRL-RX-WP-JA-2016-0274

12. DISTRIBUTION/AVAILABILITY STATEMENT
Distribution Statement A. Approved for public release: distribution unlimited.

13. SUPPLEMENTARY NOTES
PA Case Number: 88ABW-2015-3614; Clearance Date: 15 Jul 2015. This document contains color. Journal article published in Materials Science & Engineering A, Vol. 648, 11 Nov 2015. © 2015 Elsevier Ltd. The U.S. Government is joint author of the work and has the right to use, modify, reproduce, release, perform, display, or disclose the work.
The final publication is available at http://dx.doi.org/10.1016/j.msea.2015.09.080

14. ABSTRACT *(Maximum 200 words)*
High-resolution electron backscatter diffraction (EBSD) was used to examine the grain structure in long rods of ultrafine-grain (UFG)commercial-purity titanium produced for medical implants. The UFG material was obtained by equal channel angular pressing (ECAP) using a Conform scheme followed by rod drawing. The microstructure was found to be bimodal consisting of relatively coarse elongated grains containing well-developed substructure and ultrafine grains. The mean grain size was 0.3 μm, and the fraction of high-angle boundaries was 45%. The material had a strong <101¯0>-fiber texture. An analysis of the microstructure–properties relationship showed that the increase in material strength developed during severe plastic deformation resulted from grain refinement and substructure evolution in comparable measure.

15. SUBJECT TERMS
EBSD; Titanium alloys; Nanostructured materials; Equal channel angular processing; Grain refinement

16. SECURITY CLASSIFICATION OF:			17. LIMITATION OF ABSTRACT:	18. NUMBER OF PAGES	19a. NAME OF RESPONSIBLE PERSON (Monitor)
a. REPORT	b. ABSTRACT	c. THIS PAGE			Bill Song
Unclassified	Unclassified	Unclassified	SAR	9	19b. TELEPHONE NUMBER *(Include Area Code)* (937) 255-1351

REPORT DOCUMENTATION PAGE Cont'd

6. AUTHOR(S)

3) S.Mironov - Tohoku University

4) S.L. Semiatin - AFRL/RX

7. PERFORMING ORGANIZATION NAME(S) AND ADDRESS(ES)

3) Tohoku University, 6-6-02 Aramaki-aza-Aoba,
Sendai 980-8579, Japan

4) AFRL/RX Wright Patterson AFB, OH 45433

Materials Science & Engineering A 648 (2015) 305–310

Contents lists available at ScienceDirect

Materials Science & Engineering A

journal homepage: www.elsevier.com/locate/msea

An EBSD investigation of ultrafine-grain titanium for biomedical applications

G.S. Dyakonov [a,b], E. Zemtsova [b,c], S. Mironov [d,*], I.P. Semenova [a], R.Z. Valiev [b], S.L. Semiatin [e]

[a] Institute of Physics of Advanced Materials, Ufa State Aviation Technical University, 12K Marx St., Ufa 450000, Russia
[b] Laboratory for Mechanics of Bulk Nanostructured Materials, Saint Petersburg State University, 26 Universitetsky Prospect, 198504 Peterhof, Saint Petersburg, Russia
[c] Institute of Chemistry, Saint Petersburg State University, 26 Universitetsky Prospect, Saint Petersburg 198504, Russia
[d] Department of Materials Processing, Graduate School of Engineering, Tohoku University, 6-6-02 Aramaki-aza-Aoba, Sendai 980-8579, Japan
[e] Air Force Research Laboratory, Materials and Manufacturing Directorate, AFRL/RXCM, Wright-Patterson AFB, OH 45433-7817, USA

ARTICLE INFO

Article history:
Received 11 July 2015
Received in revised form
11 September 2015
Accepted 17 September 2015
Available online 21 September 2015

Keywords:
EBSD
Titanium alloys
Nanostructured materials
Equal channel angular processing
Grain refinement

ABSTRACT

High-resolution electron backscatter diffraction (EBSD) was used to examine the grain structure in long rods of ultrafine-grain (UFG) commercial-purity titanium produced for medical implants. The UFG material was obtained by equal channel angular pressing (ECAP) using a Conform scheme followed by rod drawing. The microstructure was found to be bimodal consisting of relatively coarse elongated grains containing well-developed substructure and ultrafine grains. The mean grain size was ~0.3 μm, and the fraction of high-angle boundaries was ~45%. The material had a strong <10$\bar{1}$0>-fiber texture. An analysis of the microstructure–properties relationship showed that the increase in material strength developed during severe plastic deformation resulted from grain refinement and substructure evolution in comparable measure.

1. Introduction

Due to excellent biocompatibility, commercial-purity titanium is a very attractive material for orthopedic and dental applications. However, the use of ordinary coarse-grain titanium is limited by its relatively low strength. To increase its strength to a desirable level, a two-step approach has been developed recently [1–6]. The method is based on severe plastic deformation (SPD) and typically includes warm equal-channel angular pressing (ECAP) followed by ether cold rolling, axisymmetric extrusion, or rod drawing. The strengthening developed during the two-step approach is commonly accepted to originate from extensive grain refinement to the ultrafine range. To obtain the desired properties in a repeatable fashion, however, careful microstructure control is necessary.

To date, microstructural examinations in such materials have usually been performed using transmission electron microscopy (TEM) and x-ray measurements [1–3,5,6]. These investigations have revealed the formation of a fine-grain structure with a mean size of ~0.2 μm, high dislocation density, and a relatively-strong crystallographic texture. However, several important characteristics of the grain structure, in particular the grain-boundary character, are still unclear, thus hampering the development of quantitative microstructure–property relationships. To establish this relationship, high-resolution electron-backscatter diffraction (EBSD) was employed in the present work for a thorough characterization of the severely-deformed microstructure. The results of these measurements were used to elucidate the discrete contributions of grain refinement, dislocations, and solid–solution elements to the yield strength.

2. Material and experimental procedures

The material used in the present investigation was commercial-purity titanium (CP Ti) Grade 4 whose chemical composition is given in Table 1. In the as-received condition, it had an equiaxed grain size of ~25 μm.

The program material was subjected to ECAP via route B_C using a Conform scheme [6,7]. This technique enables the production of an ultrafine microstructure in billets of long length (to several meters) and is suitable for commercial-production applications. In the present investigation, ECAP-Conform was performed on samples measuring 11 × 11 mm^2 in cross section and 500 mm length at 250 °C to an accumulated true strain of ~4.2 (6 passes) using a die with a 120° square channel. The ram speed was 33 mm/s. After ECAP, the material was drawn at 200 °C to a total area reduction of

* Corresponding author.
E-mail address: smironov@material.tohoku.ac.jp (S. Mironov).

http://dx.doi.org/10.1016/j.msea.2015.09.080
0921-5093/

Table 1
Chemical composition (wt%) of the program material.

Ti	Fe	C	O	N	H
Balance	0.16	0.046	0.33	0.005	0.0034

Table 2
Details of EBSD measurements.

Scan step size (μm)	Map size (μm^2)	Number of pixels	Number of grains
Longitudinal section			
0.15	180 × 160	1,478,169	18,305
0.05	75 × 75	2,600,367	18,270
0.05	65 × 50	1,502,751	14,438
Transverse section			
0.05	57 × 55	1,449,355	15,472

~76% at a speed of 60 mm/s using a die with an included angle of 12°. The total area reduction was achieved using 5 passes of ~20% each. By this means, a finished rod with a diameter of 6 mm was obtained. Additional details of the SPD process are summarized elsewhere [6].

Microstructure characterization was performed primarily by EBSD. To provide a 3-dimensional view of the grain structure, samples were cut from both longitudinal and transverse cross sections of the final rods. EBSD specimens were prepared using conventional metallographic techniques followed by long-term (24 h) vibratory polishing with a colloidal-silica suspension. In all cases, microstructural observations focused on the central part of the rods. EBSD analysis was conducted with a JSM-7800 F field-emission gun, scanning electron microscope (FEG–SEM) equipped with a TSL OIM^{TM} EBSD system. To examine the microstructure at different length scales, EBSD maps were acquired with a scan step size of 0.05 or 0.15 μm (Table 2). For each diffraction pattern, nine Kikuchi bands were used for indexing, thus minimizing the possibility of errors. To improve the reliability of the EBSD data, grains comprising three or fewer pixels were automatically cleaned from the maps using the grain-dilation option in the TSL software. Furthermore, to eliminate spurious boundaries caused by orientation noise, a lower-limit boundary misorientation cut-off of 2° was used. A 15° criterion was applied to differentiate low-angle boundaries (LABs) and high-angle boundaries (HABs).

Because real microstructures sometimes exhibit a complex mixture of LABs and HABs, confusion can arise with regard to the definition of grains. To avoid this ambiguity, the term "grain" in the present work was applied to denote a crystallite bordered by a *continuous* HAB perimeter.

Two approaches were used to quantify the grain size per se. The first was the classical, linear-intercept method. Because this technique does not account for the *volume fraction* of grains with different sizes, the so-called grain-reconstruction method was also applied [8]. In this technique, the grain size is quantified by the measured grain area (in a 2-dimensional section) and the calculation of the equivalent grain diameter assuming each grain as a circle.

3. Results

3.1. Microstructure observations

Longitudinal and transverse EBSD inverse-pole-figure (orientation) maps revealed the grain structure developed during ECAP/rod drawing (Fig. 1). In the maps, LABs and HABs are depicted by white and black lines, respectively.

At relatively-low magnification (Fig. 1a), the microstructure appeared to consist primarily of relatively-coarse, elongated grains aligned with the drawing direction. The grain length often exceeded 25 μm, whereas the thickness was only several microns. By and large, the grain shape mirrored the deformation imposed during the rod-drawing steps of the process, thereby suggesting that the observed grain structure probably originated from the geometric effect of strain per se.

At much higher magnification (Fig. 1b, c), on the other hand, it was evident that the microstructure also contained fine grains (≤ 1 μm) and was thus somewhat bimodal in nature. The higher-magnification EBSD results also indicated that the coarse elongated grains contained developed substructure. In this substructure, some sub-boundary segments exhibited misorientations *above* 15° (e.g., boundaries indicated by arrows in Fig. 1b and c), thus suggesting a gradual LAB-to-HAB transformation during straining. Furthermore, in some locations, the deformation-induced HABs delimited microstructural entities almost completely (areas indicated by rectangles in Fig. 1b and c); such features also appeared to indicate a gradual transition from subgrains to grains.

In terms of morphology and dimensions, the partially-transformed subgrains were broadly similar to the typical fine grains observed elsewhere in the microstructure. These observations thus indirectly indicate that grain refinement probably occurred via *continuous* dynamic recrystallization. Considering the relatively-low processing temperature (~$0.24T_m$, where T_m is melting point), this hypothesis is reasonable. Nevertheless, its confirmation requires more-detailed examination of microstructure evolution at different levels of accumulated strain.

It was also found that the fine grains were not distributed randomly throughout the microstructure but tended to cluster near original grain boundaries (Fig. 1b and c). The preferential grain refinement in these areas was surmised to be associated with relatively high local strains generated at grain boundaries.

3.2. $\alpha \rightarrow \omega$ martensitic phase transformation

It has been reported that SPD at relatively high imposed levels of stress (order of several GPa) may induce an $\alpha \rightarrow \omega$ martensitic phase transformation in titanium [9–12]. For the rod processed by ECAP/drawing in the present effort, EBSD measurements (Fig. 2) revealed the presence of a very small fraction (~3.5 vol%) of the ω phase. The ω phase comprised fine (~0.15 μm) nearly-equiaxed particles along grain boundaries in the α phase (Fig. 2). Therefore, the $\alpha \rightarrow \omega$ phase transformation did appear to make a contribution, albeit small, to the formation of the fine-grain microstructure shown in Fig. 1b and c. However, the α and ω phases have similar hexagonal crystal structures and thus mis-indexing could have occurred during EBSD analysis. Therefore, additional study is necessary to verify these observations.

Assuming the Orowan mechanism, the magnitude of the strength increment due the omega phase was estimated to be very small (i.e., ~10 MPa), and thus it was ignored in the present work.

3.3. Grain size of the α phase

The size of the α grains quantified by the linear-intercept and grain-reconstruction methods revealed some noticeable differences (Fig. 3a and b). For the linear-intercept approach, only the grain *thickness* was measured, i.e. the HAB spacing in a direction perpendicular to the axis of the drawn rod.

The mean grain size of the α phase measured by the intercept method was ~0.4 μm in the longitudinal cross section and ~0.3 μm in the transverse section (Fig. 3a). Therefore, the grain size of the ECAP/drawn rod fit the typical definition for ultrafine-grain materials. When all of the EBSD-detected boundaries (i.e.,

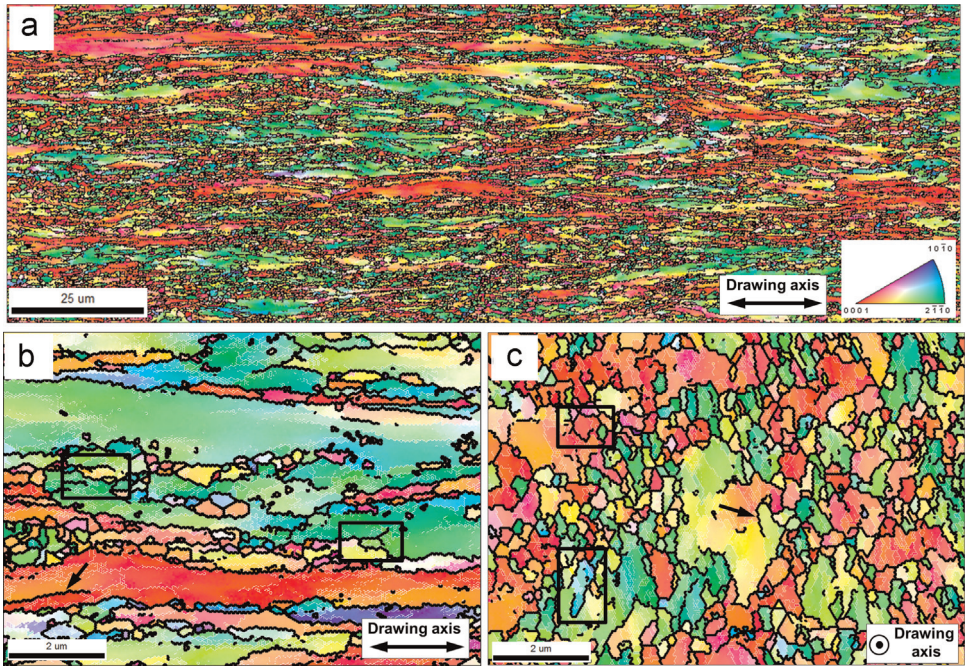

Fig. 1. Selected portions of EBSD inverse-pole-figure maps for the radial direction showing the microstructure in (a, b) longitudinal and (c) transverse cross sections of the severely-deformed final rod. In the maps, LABs and HABs are depicted as white and black lines, respectively. For simplicity, only HABs are shown in (a).

those with misorientations above 2°) were included in the analysis, the mean intercept length was determined to be ~0.15 μm. This value is very close to that based on TEM observations reported in literature [1–3,5,6].

It should be stressed that the volume fraction of coarse grains (≥ 1 μm) was high (Fig. 3b). Not surprisingly, the area fraction of such grains measured in longitudinal cross section was substantially higher than that observed in the transverse section (i.e., 78% vs 54%). This observation can be rationalized on the basis of the preferential concentration of fine grains along the boundaries of the coarse elongated grains (Fig. 1b and c). Indeed, due to the elongated-shape of the coarse grains, the specific area of their boundaries in transverse cross sections should be *larger* than in longitudinal sections. Correspondingly, the volume fraction of fine grains should appear relatively high in transverse sections as was observed.

3.4. Texture of the α phase

The EBSD orientation data for the α phase were used to derive an inverse pole figure for the drawing direction (Fig. 4). These results indicated that a strong texture consisting of $<10\bar{1}0>$ //drawing axis (i.e., a $<10\bar{1}0>$-fiber texture) had been formed. This observation agrees well with x-ray measurements of the same material [6] and is as expected for cold-drawn α titanium [13].

The critical resolved shear stress for plastic deformation of α titanium is lowest for prism slip ($\{10\bar{1}0\} < 11\bar{2}0>$), intermediate for basal slip ($[0001] < 11\bar{2}0>$), and highest for pyramidal ⟨c+a⟩ slip. Thus, the development of an *ideal* $<10\bar{1}0>$-fiber texture indicated that *on average* 2 of the 3 prism slip planes/systems were likely activated symmetrically in most of the crystallites (relative to the drawing direction), thereby leading to a stable orientation for most of the grains, for which the Schmid factor would be

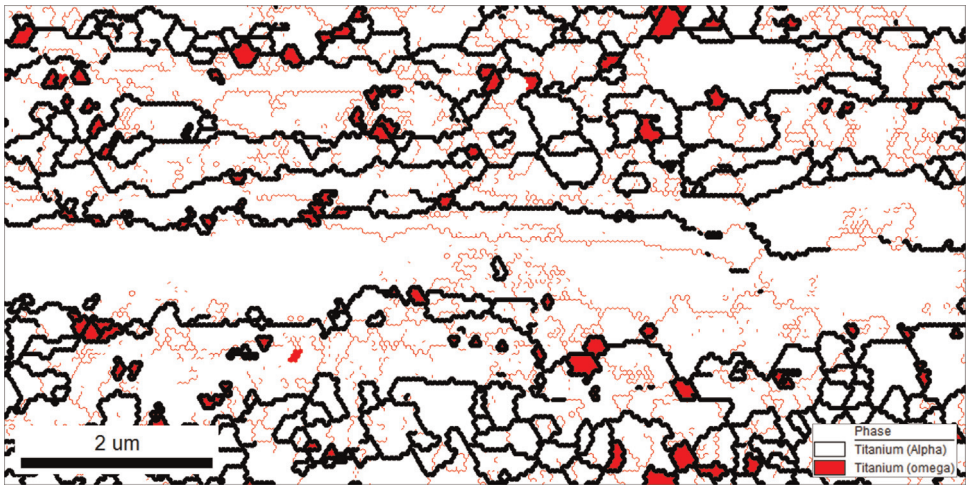

Fig. 2. Selected portion of an EBSD map for the alpha (white) and omega (red) phases taken from the longitudinal cross section of severely-deformed rod. In the map, LABs and HABs are depicted as red and black lines, respectively. (For interpretation of the references to color in this figure legend, the reader is referred to the web version of this article.).

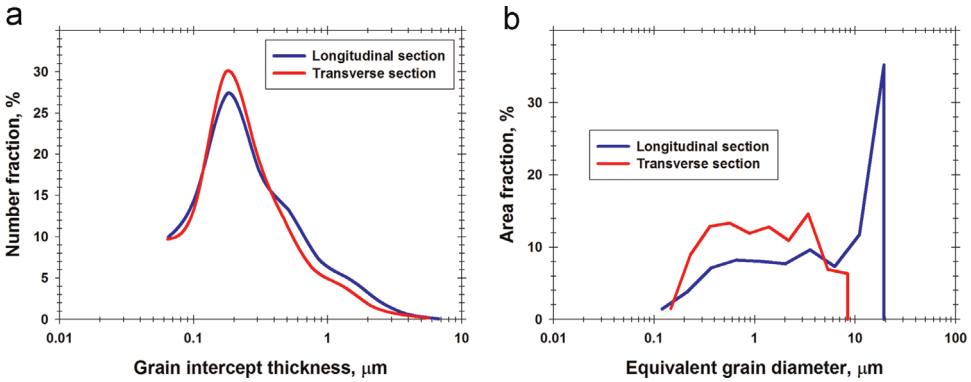

Fig. 3. Grain-size distributions for the α phase: (a) Grain-intercept thickness and (b) equivalent grain diameter.

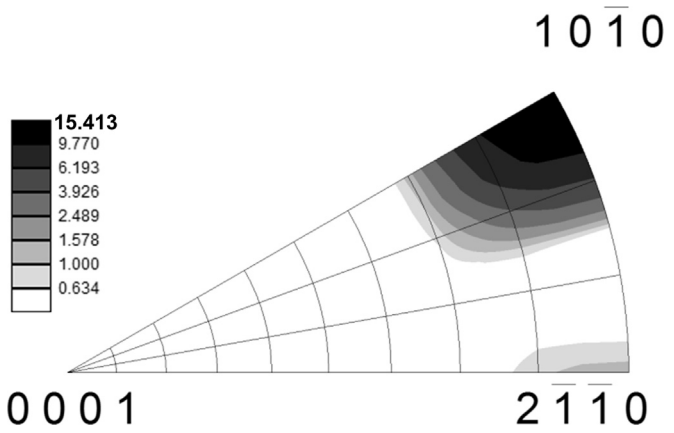

Fig. 4. Inverse pole figure for the drawing direction showing the crystallographic orientations of the a phase.

$\sqrt{3}/4$[†]. For such a strong crystallographic *and* mechanical texture, the strain compatibility requirements along the longitudinal boundaries of the coarse elongated grains may have been relaxed, and the requirement for ⟨c+a⟩ slip or twinning to accommodate the radial compressive strain during drawing could have been reduced. Thus, the driving force for grain subdivision would have been expected to be low as well. In reality, however, the *measured* texture was characterized by an orientation spread (Fig. 4), and some degree of strain incompatibility would have developed across the longitudinal boundaries. This inhomogeneity was probably one of the possible sources of the observed grain refinement (Fig. 1b and c). Nevertheless, the formation of the strong <10$\bar{1}$0>-fiber texture would have retarded the refinement process and resulted in the retention of the relatively-high volume fraction of coarse, elongated grains found in the material (Fig. 3b).

In addition to the <10$\bar{1}$0>-fiber texture, a minor fraction of a <2$\bar{1}\bar{1}$0>-fiber was also observed (Fig. 4). This texture component was found to predominate in the *ω* phase. Therefore, its detection in the α phase may have resulted from indexing errors during EBSD mapping. Due to the very low volume fraction of this texture component (< 1 pct., Fig. 4), its influence on material strength was likely minimal, and thus was ignored.

3.5. Misorientation distribution of the α phase

Misorientation distributions measured in both cross sections were found to be broadly similar to each other. For the sake of brevity, therefore, only misorientations measured for the longitudinal section are shown in Fig. 5.

The misorientation-angle distribution was dominated by a low-angle peak (Fig. 5a). It should be noted the LABs were preferentially concentrated *within* the relatively-coarse elongated grains (Fig. 1b). Therefore, the observed low-angle maximum was likely attributable to the relatively slow LAB-to-HAB transformation kinetics (as discussed in Section 3.4) rather than the sharp fiber texture (Fig. 4). As expected, the HAB fraction in the transverse section was larger than that in the longitudinal section (45% vs. 39%)[‡]. With the exception of the low-angle maximum, the misorientation-angle distribution was relatively smooth with no significant peaks. In addition, almost no twin misorientations were found. This observation indicated that twinning was likely not operative during the final drawing step. Even if twins had formed at *low* strains, subsequent deformation would have destroyed the twin relationship.

In contrast to the misorientation-angle distribution per se, the misorientation-*axis* distribution was somewhat complex. Excluding the LABs, the axes were clustered near <10$\bar{1}$0>, <2$\bar{1}\bar{1}$0>, <0001>, and <4$\bar{1}\bar{3}$1> (Fig. 5b). In particular, the clustering of misorientation axes near the <10$\bar{1}$0> and <2$\bar{1}\bar{1}$0> poles was observed for almost the entire misorientation range (Fig. 5b). It is likely therefore that this effect was associated with the development of the <10$\bar{1}$0>- and <2$\bar{1}\bar{1}$0>-fiber textures (Fig. 4). For example, the formation the <10$\bar{1}$0>-fiber texture implies that the grains with <10$\bar{1}$0 > //drawing axis were rotated arbitrarily about the drawing direction.

The cluster near ⟨0001⟩ mainly comprised HABs with 15°–30° misorientations (Fig. 5b). As shown previously [14,15], this effect in severely deformed α titanium may be attributed to dislocation boundaries originating from predominantly prism slip. The cluster of rotation axes near <4$\bar{1}\bar{3}$1> was produced by the HABs with highest possible misorientations (Fig. 5b). Their origin is not clear and requires additional study.

4. Discussion

EBSD measurements enabled the detailed characterization of the grain structure in UFG titanium. Based on these data (and pertinent results in the published literature), the specific contribution of various mechanisms to the overall strength of UFG titanium have been quantified and are discussed in this section.

Assuming that different strengthening mechanisms act independently and thus are additive in nature, the yield strength can be expressed as the following:

[†] The *measured* average Schmid factor for prism slip was 0.45

[‡] In some respects, the criterion for the LAB-to-HAB transition is subjective. Assuming a 10° criterion for differentiation of LABs and HABs, the HAB proportion was 52% in the longitudinal section and 62% in the transverse section.

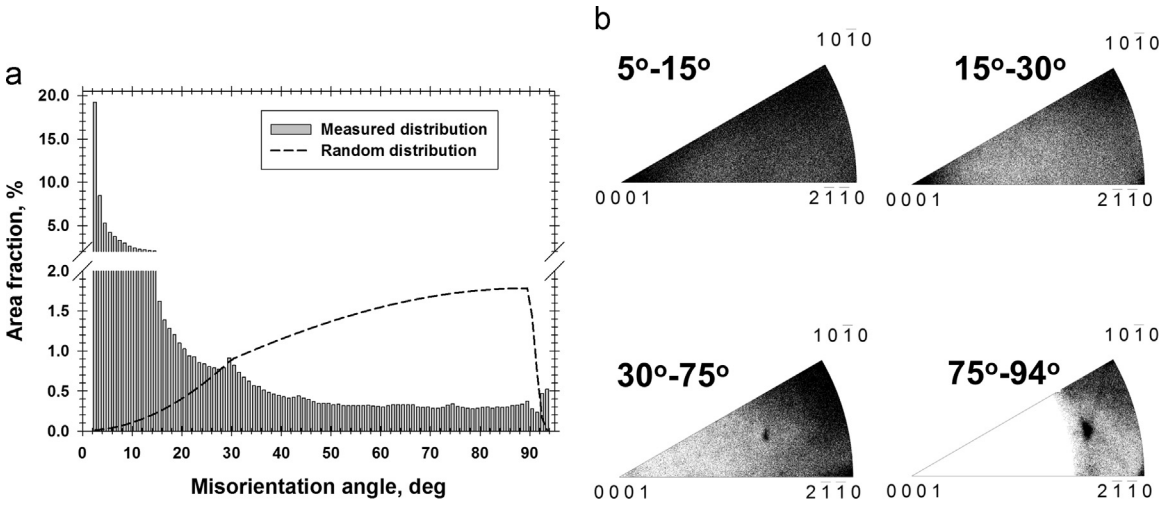

Fig. 5. Typical distributions of (a) misorientation angle and (b) misorientation axis.

$$\sigma = \sigma_0 + \sigma_g + \sigma_s \quad (1)$$

in which σ_0, σ_g, and σ_s denote the friction stress, the grain-refinement strengthening, and the strength increment due to substructure, respectively.

4.1. Friction stress due to solid–solution strengthening

In commercial-purity titanium, the friction stress is dominated by solid–solution strengthening, which in turn is controlled by the content of the interstitial solutes oxygen, nitrogen, and carbon [13]. The total interstitial content is sometimes converted to an oxygen equivalent via simple summation of the fractions of these elements. For the present material, the oxygen equivalent was ~0.4 wt% (Table 1) or ~1 at%. At ambient temperature, the friction stress for this level of interstitials was estimated to be approximately 425 MPa [13].

4.2. Grain-boundary strengthening

The strength increment associated with grain boundaries was described using the conventional Hall–Petch (HP) relation. However, because of the bimodal nature of the grain microstructure (Fig. 1b, c), the total HP strength was formulated as the sum of the contributions from the coarse grains (σ_{CG}) and the fine grains (σ_{FG}), i.e.

$$\sigma_g = \sigma_{CG} + \sigma_{FG} = k_{HP}[f_{CG} d_{CG}^{-0.5} + (1 - f_{CG}) d_{FG}^{-0.5}] \quad (2)$$

Here, k_{HP} is Hall–Petch constant (~0.3 MPa × $m^{0.5}$ at ambient temperature [13]), f_{CG} is volume fraction of the coarse grains (0.54), and d_{CG} and d_{FG} denote the mean thicknesses of the coarse and fine grains, respectively (i.e., 1.7 μm and 0.3 μm, respectively). The calculated grain-boundary strengthening is shown in Table 3.

It should be pointed out that the Hall–Petch constant k_{HP} used in the present calculations (0.3 MPa × $m^{0.5}$) was obtained for *coarse-grain* titanium [13], which is prone to mechanical twinning.

Table 3
Contribution of strengthening mechanisms.

Predicted strengthening (MPa)					Measured yield strength (MPa) [6]
Friction stress	HABs	Dislocations	LABs	Total	
425	340	146	311	1222	1190

Twinning is believed to reduce k_{HP} in commercial-purity titanium [16]. In the present UFG material, however, twinning was suppressed, and thus the grain-boundary strengthening may be larger than that predicted above (Table 3). For instance, for a Hall–Petch constant of 0.4 MPa × $m^{0.5}$, the strength increment would be ~450 MPa.

4.3. Substructure strengthening

Substructure strengthening results from free (mobile) dislocations as well as low-angle (dislocation-) boundaries within the grains defined by HABs. It can thus be expressed as the following

$$\sigma_s = \sigma_d + \sigma_{LAB} \quad (3)$$

Dislocation strengthening is usually described by the classic Taylor relation:

$$\sigma_d = M\alpha G b \rho^{0.5} \quad (4)$$

Here, M is the Taylor factor, α is a constant of the order of 0.1–0.5 [13] (taken to be 0.15 in the present work), G denotes the shear modulus of titanium (~40 GPa), b is the Burgers vector (=0.295 nm for $<a>$ dislocations), and ρ is the density of free dislocations.

As mentioned above, the critical resolved shear stress for the different slip systems in hcp titanium varies considerably, and thus the evaluation of the Taylor factor can be challenging. However, in light of the relaxed degree of constraint due to the formation of an elongated grain structure with a sharp <10$\bar{1}$0>-fiber texture, the material flow along the drawing direction is dominated by prism slip, as discussed in Section 3.4. For uniaxial tension along the drawing axis and the predominance of the prism slip, the mean Taylor factor was calculated to be 2.6.

The heavily-deformed titanium was characterized by large internal stresses, and thus the direct measurement of the dislocation density ρ was not possible. Nevertheless, recent x-ray estimates have suggested that it may be as high as ~10^{15} m^{-2}[6]. Hence, ρ was taken to be ~10^{15} m^{-2} in the present work.

In contrast to HABs, low-angle (dislocation) boundaries are assumed to be penetrable by slip and thus contribute to the overall strength via forest-like hardening. In such cases, the strengthening contribution of LABs is given by the following relation [17]:

$$\sigma_{LAB} = (M\alpha G\sqrt{3b\theta_{LAB}f}) \times d_{SG}^{-0.5} \quad (5)$$

in which θ_{LAB} denotes the mean LAB misorientation, f is the LAB fraction, and d_{SG} is the mean subgrain size. Unfortunately,

EBSD cannot reliably detect misorientations below 2°, therefore, accurate measurement of these three characteristics is difficult. Neglecting very low-angle boundaries, however, the mean LAB misorientation was found to be 7° (0.122 rad); the LAB fraction was 0.55, and the mean subgrain size was 0.15 μm. It should be pointed out that the present method tends to lead of course to an *overestimate* of the strengthening associated with LABs.

The calculated strength increments associated with dislocations and LABs are listed in Table 3.

4.4. Microstructure–strength relationship

Table 3 summarizes the contributions of the different strengthening mechanisms to the yield strength of the final product produced by ECAP+drawing. Summing these values resulted in a yield-strength prediction very close to the measured value.

The calculations in Table 3 also revealed that substructure strengthening is comparable in magnitude to that due to the Hall–Petch effect. The relatively-low HAB strengthening can rationalized on the basis of the retention of a significant volume fraction of coarse grains in the microstructure (Figs. 1a, 3b) and suggests that the already high strength level achieved in the present UFG titanium can be further improved. Nevertheless, the results do indicate that the creation of well-developed substructure may be sufficient to impart a desirable modicum of strength to commercial-purity titanium. That is to say, there may be no need to complete the LAB-to-HAB transformation.

5. Summary

High-resolution EBSD was applied to examine the grain structure, texture, and misorientation distribution developed in ultrafine-grain, commercial-purity titanium for biomedical applications. The material was produced using a two-step approach involving ECAP-Conform at 250 °C to a total true strain of 4.2 followed by drawing at 200°C to an area reduction of 76%. The main conclusions from this work are as follows.

(1) The final grain structure was bimodal consisting of relatively-coarse (≥ 1 μm) heavily-deformed, elongated grains surrounded by necklaces of fine, equiaxed grains. Although the mean grain thickness was ~0.3 μm, the microstructure was characterized by a relatively-large volume fraction ($\geq 55\%$) of retained coarse grains. Assuming a 15° criterion to differentiate LABs and HABs, the HAB fraction was found to be ~45%.
(2) Texture was dominated by a strong <10$\bar{1}$0>-fiber. This texture was deduced to retard the grain-refinement process.
(3) The formation of the observed microstructure was hypothesized to be attributable to the geometric effect of strain and continuous dynamic recrystallization. No significant evidence of twinning was found. On the other hand, it is possible that a small volume fraction of the material (~3.5%) had undergone an α→ω martensitic phase transformation.
(4) The contribution of substructure strengthening (due to dislocations and LABs) to the final material strength developed during SPD was found to be comparable to that due to the formation of a UFG microstructure.

Acknowledgments

R.Z. Valiev gratefully acknowledges the support from the Russian Federal Ministry for Education and Science (RZV Grant no. 14. B25.31.0017), and I.P. Semenova acknowledges the support of the said Ministry within the scope of the basic part of the State Assignment. This work was also supported in part by a grant from the Saint Petersburg State University No 6.37.431.2015.

References

[1] V.V. Stolyarov, Y.T. Zhu, I.V. Alexandrov, T.C. Lowe, R.Z. Valiev, Grain refinement and properties of pure Ti processed by warm ECAP and cold rolling, Mater. Sci. Eng. A 343 (2003) 43–50.
[2] V.V. Stolyarov, L. Zeipper, B. Mingler, M. Zehetbauer, Influence of post-deformation on CP-Ti processed by equal channel angular pressing, Mater. Sci. Eng. A 476 (2008) 98–105.
[3] Z. Fan, H. Jiang, X. Sun, J. Song, X. Zhang, C. Xie, Microstructures and mechanical deformation behaviors of ultrafine-grained commercial pure (grade 3) Ti processed by two-step severe plastic deformation, Mater. Sci. Eng. A 527 (2009) 45–51.
[4] D.-H. Kang, T.-W. Kim, Mechanical behavior and microstructural evolution of commercially pure titanium in enhanced multi-pass equal channel angular pressing and cold extrusion, Mater. Des. 31 (2010) 54–60.
[5] I. Sabirov, M.T. Perez-Prado, J.M. Molina-Aldareguia, I.P. Semenova, G. Kh Salimgareeva, R.Z. Valiev, Anisotropy of mechanical properties in high-strength ultra-fine-grained pure Ti processed via a complex severe plastic deformation route, Scr. Mater. 64 (2011) 69–72.
[6] D.V. Gunderov, A.V. Polyakov, I.P. Semenova, G.I. Raab, A.A. Churakova, E. I. Gimaltdinova, I. Sabirov, J. Segurado, V.D. Sitdikov, I.V. Alexandrov, N. A. Enikeev, R.Z. Valiev, Evolution of microstructure, macrotexture and mechanical properties of commercially-pure Ti during ECAP-conform processing and drawing, Mater. Sci. Eng. A 562 (2013) 128–136.
[7] G.J. Raab, R.Z. Valiev, T.C. Lowe, Y.T. Zhu, Continuous processing of ultrafine grained Al by ECAP–Conform, Mater. Sci. Eng. A 382 (2004) 30–34.
[8] F.J. Humphreys, Quantitative metallography by electron backscattered diffraction, J. Microsc. 195 (1999) 170–185.
[9] Y. Todaka, J. Sasaki, T. Moto, M. Umemoto, Bulk submicrocrystalline ω-Ti produced by high-pressure torsion straining, Scr. Mater. 59 (2008) 615–618.
[10] M. Tane, Y. Okuda, Y. Todaka, H. Ogi, A. Nagakubo, Elastic properties of single-crystalline ω phase in titanium, Acta Mater. 61 (2013) 7543–7554.
[11] K. Edalati, T. Daio, M. Arita, S. Lee, Z. Horita, A. Togo, I. Tanaka, High-pressure torsion of titanium at cryogenic and room temperatures: grain size effect on allotropic phase transformations, Acta Mater. 68 (2014) 207–213.
[12] M. Shirooyeh, J. Xu, T.G. Langdon, Microhardness evolution and mechanical characteristics of commercial-purity titanium processed by high-pressure torsion, Mater. Sci. Eng. A 614 (2014) 223–231.
[13] H. Conrad, Effect of interstitial solutes on the strength and ductility of titanium, Prog. Mater. Sci. 26 (1981) 123–403.
[14] S. Yu Mironov, G.A. Salishchev, M.M. Myshlyaev, R. Pippan, Evolution of misorientation distribution during warm '*abc*' forging of commercial-purity titanium, Mater. Sci. Eng. A 418 (2006) 257–267.
[15] G.S. Dyakonov, S. Mironov, S.V. Zherebtsov, S.P. Malysheva, G.A. Salishchev, A. A. Salem, S.L. Semiatin, Grain-structure development in heavily cold-rolled alpha-titanium, Mater. Sci. Eng. A 607 (2014) 145–154.
[16] N. Stanford, U. Carlson, M.R. Barnett, Deformation twinning and the Hall–Petch relation in commercial purity Ti, Metal. Mater. Trans. A 39A (2008) 934–944.
[17] N. Hansen, Hall–Petch relation and boundary strengthening, Scr. Mater. 51 (2004) 801–806.